Article

Never-Ending Story: New Cyclodextrin-Based Metal−Organic Framework Crystal Structures Obtained Using Different Crystallization Methods

Kristīne Krūkle-Bērziņa* and Anatoly Mishnev

Read Online

ACCESS | Metrics & More | Article Recommendations | SI Supporting Information

ABSTRACT: Six novel cyclodextrin (CD)-based metal−organic frameworks (MOFs) were synthesized using distinct crystallization methodologies. A modified vapor diffusion method is introduced for the first time, termed fast crystallization, which enables the rapid solid-state formation of MOF compounds. This innovative method yielded four of the newly synthesized MOFs. The crystal structures of five obtained frameworks were structurally characterized through single-crystal X-ray diffraction, while one, compound **5** (γ-CD-K-5), was additionally characterized as a bulk powder. Structural analysis revealed that two of the newly obtained MOFs, namely, compound **2** (α-CD-K-2) and compound **3** (α-CD-Rb-3), exhibited isostructural characteristics, forming a three-dimensional (3D) framework. Compound **1** (α-CD-K-1) shared the same space group as EVEGET (α-CD-K) and displayed the same framework type. Furthermore, the crystal packing of compound **4** (β-CD-K-4) closely resembled that of compound **1** and EVEGET, with the only distinction lying in the type of CD employed. Notably, compound **6** (γ-CD-K-6) incorporated an iodine ion with an occupancy of 0.2. To discern the intermolecular interactions within the obtained MOFs, the Hirshfeld surface was calculated using Crystal Explorer software.
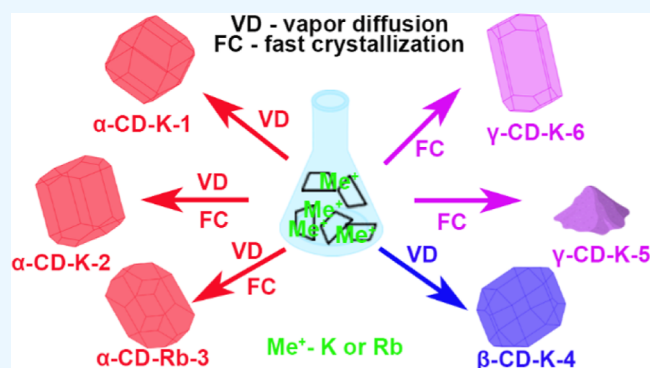
1. INTRODUCTION

Metal−organic frameworks (MOFs) have been known for decades, and they have continuously gained interest because of their increasing application potential in various fields—pharmacy, medicine, technology, ecology, etc.[1] MOFs are considered promising drug carriers because of their porous architecture and adjustable properties, which can be used for drug loading and more controlled release in simulated physiological conditions.[2] Modification of the properties of an existing active pharmaceutical ingredient (API) without changing its biological role can be much faster and more effective than creating new drugs from scratch.[3]

In the role of a drug carrier, it is imperative that MOFs exhibit biocompatibility. To achieve this, biologically acceptable metals—Ca, Fe, K, and Na[4,5]—and a nontoxic ligand should be used in the MOF synthesis process. Cyclodextrin (CD) has emerged as an ideal ligand candidate because of its chemical and physical stability. CD represents a cyclic oligosaccharide derived from the enzymatic degradation of starch, with α, β, and γ configurations being the most prevalent naturally occurring forms, comprising 6, 7, and 8 glucopyranose units, respectively.[6,7]

A growing interest in the use of various CDs in MOFs arose after Stoddart et al.[8] published the first method of CD MOF obtaining.[9,10] The diffusion method using methanol diffusion in water solution is the main method for obtaining CD MOFs.[8] It is possible to obtain high-quality crystals, but it is a time-consuming process.[5] Consequently, modifications such as the incorporation of additional surfactants such as CTAB[5] or PEG[11] are employed to facilitate the production of CD MOF nanoparticles.[12] An alternative method employed for MOF synthesis is the solvothermal approach, which is exemplified by the synthesis of β-CD-Cs.[13,14] It is possible to use cogrinding, but there are still only a few publications and, in most cases, an amorphous phase of the CD MOF has been obtained.[15]

The most studied and well-known CD MOF is γ-CD-K (LAJLAL) α phase;[8] as shown in Table 1, it crystallizes into a cubic crystal system occupying space group $I432$. It is built up from the $(\gamma$-CD$)_6$ cube. LAJLAL is isomorphic with γ-CD-Rb (LAJLEP) and γ-CD-Cs (LAJKULE). Moreover, γ-CD-K exhibits multiple crystal phases, including the trigonal β phase (LAJLAL02),[9] which crystallizes in space groups $R32$, ε (orthorhombic, $I222$), and δ (tetragonal, $I4$).[16] The iso-

Table 1. Summary of the CD Based on the First Group Elements' MOF Crystal Lattice and the Unit Cell Parameters[a]

Identification	CD	Metal	Space group	a, Å	b, Å	c, Å	α, °	β, °	γ, °	V, Å3
EVEGET[20]	α	K	$P2_1$	13.813	33.186	13.971	90	118.69	90	5618.0
KOBRIC/PULLUF	β	K	$P2_1$	15.223	10.578	20.204	90	108.37	90	3087.6
YAMVIV[21]	β	K	$P2_12_12_1$	14.751	23.686	40.870	90	90	90	14279
LAJLAL	γ	K	$I432$	31.006	31.006	31.006	90	90	90	29808
LAJLAL02	γ	K	$R32$	43.6764	43.6764	28.1864	90	90	120	46565
ZUGDEN	γ	K	$I222$	15.7898	20.2381	28.1282	90	90	90	8988.5
ZUGDIR	γ	K	$I4$	23.80929	23.8092	15.2629	90	90	90	8652.3
TOHXIA[22]	γ	K	$P2_12_12_1$	10.9064	30.793	22.920	90	90	90	7417.9
OXUWIP[23]	α	Na	$P2_12_12_1$	11.5783	15.9764	26.6031	90	90	90	4921.0
PULLOZ	β	Na	$P2_1$	15.237	10.596	20.202	90	108.224	90	3098.0
ZUNVEL[24]	β	Na	$P2_12_12_1$	10.353	19.678	29.79	90	90	90	6069.0
YAPROY	γ	Na	$P1$	15.095	16.824	17.09	90.40	97.417	97.63	4264.4
LAJLEP	γ	Rb	$I432$	31.079	31.079	31.079	90	90	90	30019
MAMVED[25]	α	Rb	$P4_32_12$	27.1653	27.1653	37.9051	90	90	90	27972
LAJKUE	γ	Cs	$I432$	30.868	30.868	30.868	90	90	90	29412
SATYAQ	β	Cs	$C2$	21.981	25.367	15.79	90	133.554	90	6380.7
SAZQIW	β	Cs	$P2_1$	15.026	15.265	15.12	90	119.193	90	3027.5
YAPRUE	γ	Cs	$I4$	24.136	24.136	15.454	90	90	90	9002.6

[a]Same color indicates isostructural compounds.

morphism extends to γ-CD-Cs (YAPRUE) and γ-CD-K (ZUGDIR)[16] δ phases. In the monoclinic crystal system, β-CD-K (KOBRIC)[17] and β-CD-Na (PULLOZ)[18] similarly exhibit isomorphism, occupying the space group $P2_1$. A recent publication[19] introduced a novel γ-CD-K MOF structure that crystallizes in an orthorhombic crystal system, occupying the space group $P2_12_12$—an unreported crystal system for γ-CD MOFs before. Summarizing the abundance of isostructural relationships among these structures suggests that each CD crystallizes in any crystal system independent of the metal ions in the structure. The key determinant lies in identifying the appropriate crystallization conditions to yield the desired phase. Consequently, the potential for obtaining various CD MOF phases remains plausible and awaits exploration.

In this study, novel CD MOFs were crystallized using different methods. We modified the vapor diffusion method in this study for the first time, which allowed us to obtain the MOF immediately and quickly. The characterization of the new CD MOF crystal structures was performed using X-ray methods. We characterized the crystal structures of the five newly obtained crystal phases. One crystal phase (compound **1**) was obtained only once. We measured the single-crystal structure, but repeated experiments failed to obtain it. Therefore, it was not possible to characterize compound **1** using other methods. For one sample (compound **5**), we obtained only a powder solid; therefore, it is impossible to directly describe its structure. In addition, we characterized the thermal and architectural stabilities of the newly obtained

compounds by differential scanning calorimetry and in various solvents. Nitrogen adsorption-desorption analyses were performed for the obtained compounds. Hirshfeld surface calculations were performed to compare the obtained intermolecular contacts.

2. EXPERIMENTAL PART

2.1. Materials and Reagents. CD (α-, β-, and γ-CD, analytical-grade) was purchased from *abcr* GmbH. Sodium hydroxide, rubidium hydroxide hydrate, potassium hydroxide, potassium carbonate, potassium iodide, methanol, and tetrahydrofuran (THF) were commercially available and were used without further purification.

2.2. Synthesis of CD MOF. The synthetic protocol for CD MOF was adopted from the reported procedures α-CD,[20] β-CD,[18] and γ-CD.[8]

2.2.1. Vapor Diffusion Method. 2.2.1.1. α-CD-K-1 (Compound 1). α-CD (194 mg, 0.2 mmol), KOH (11 mg, 0.2 mmol), and LiOH (60 mg, 2.5 mmol) were dissolved in H_2O (4 mL). The solution was filtered through a syringe filter and decanted into separate vials. MeOH (5 mL) was allowed to diffuse slowly into the solution over a period of a week. Colorless cubic crystals suitable for X-ray crystallographic analysis were isolated, filtered, and washed with MeOH (3 × 5 mL).

2.2.1.2. α-CD-K-2 (Compound 2). α-CD (194 mg, 0.2 mmol) and K_2CO_3 (55−83 mg, 0.4−0.6 mmol) were dissolved in H_2O (4 mL). The solution was filtered through a syringe

Table 2. Crystallographic and Structural Refinement Data of 1, 2, 3, 4, and 6 Compounds[a]

compound	1 (α-CD-K)	2 (α-CD-K)	3 (α-CD-Rb)	4 (β-CD-K)	6 (γ-CD-K)
formula	$(2(C_{36}H_{60}O_{30})\cdot K_1)_n\cdot$ $0.6(CH_3OH)\cdot6.3(H_2O)\cdot$ (OH^-)	$(C_{36}H_{60}O_{30}K_2)_n\cdot$ $CH_3OH\cdot5(H_2O)\cdot$ CO_3^{2-}	$(C_{37}H_{67}O_{36}K_2)_n\cdot$ $CH_3OH\cdot5(H_2O)\cdot$ CO_3^{2-}	$(2(C_{42}H_{68}O_{36})K_2)_n\cdot$ $CO_3^{2-}\cdot15(H_2O)$	$(C_{48}H_{84}O_{44}K_2)_n\cdot CH_3OH\cdot$ $3.5(H_2O)\cdot1.8(OH^-)\cdot0.2(I^{2-})$
radiation		Cu K_α ($\lambda = 1.54184$ Å)			synchrotron ($\lambda = 0.5$ Å)
temperature, K	164(2)	150(1)	150(2)	149.99(10)	150(2)
crystal system	monoclinic	orthorhombic	orthorhombic	monoclinic	orthorhombic
space group	$P2_1$	$P2_12_12_1$	$P2_12_12_1$	$P2_1$	$P2_12_12_1$
a (Å)	14.3688(2)	13.03890(10)	13.08700(10)	15.69040(10)	10.6383(4)
b (Å)	23.0708(3)	13.95990(10)	13.9472(2)	24.6287(2)	22.6276(8)
c (Å)	16.2892(3)	28.6469(2)	28.9750(2)	18.8656(2)	30.8159(10)
γ (deg)	93.575(1)	90	90	108.6240(10)	90
volume (Å³)	5389.36(14)	5214.36(7)	5288.72(9)	6908.55(11)	7418.0(5)
Z	2	4	4	2	4
ρ_{calc} (g/cm³)	1.314	1.567	1.650	1.301	1.364
the absorption coefficient, (mm^{-1})	1.365	2.617	3.397	1.561	0.129
goodness-of-fit on F^2	1.076	1.025	1.067	1.062	1.131
R	$R_1 = 0.0708$, w$R_2 = 0.2156$	$R_1 = 0.0414$, w$R_2 = 0.1138$	$R_1 = 0.0401$, w$R_2 = 0.0986$	$R_1 = 0.0541$, w$R_2 = 0.1451$	$R_1 = 0.1528$, w$R_2 = 0.4405$
packing index	disorder	75.9%	72.5%	61.9%	disorder
V_V, Å³	1410	683	897	2057	1359
V_{SA}, %	12	2	3	17	5

[a]V_V—calculated void volume; V_{SA}—calculated solvent accessible volume.

filter and decanted into separate vials. MeOH (5 mL) was allowed to diffuse slowly into the solution over a period of a week. Colorless cubic crystals suitable for X-ray crystallographic analysis were isolated, filtered, and washed with MeOH (3 × 5 mL) (yield: 85–90%). Elemental analysis (%) calculated for $[C_{36}H_{60}O_{30}\cdot2K^+\cdot7(H_2O)\cdot1(CH_3OH)\cdot CO_3^{2-}]$: C, 35.01%; H, 6.19%. Found: C, 34.81%; H, 5.32%.

2.2.1.3. α-CD-Rb-1 (Compound 3). α-CD (194 mg, 0.2 mmol) and RbOH (55–83 mg, 0.4–0.6 mmol) were dissolved in H_2O (4 mL). The solution was filtered through a syringe filter and decanted into separate vials. MeOH (5 mL) was allowed to diffuse slowly into the solution over a period of a week. Colorless cubic crystals suitable for X-ray crystallographic analysis were isolated, filtered, and washed with MeOH (3 × 5 mL) (yield: 60–70%). $[C_{36}H_{60}O_{30}\cdot2Rb^+\cdot1(H_2O)\cdot3(CH_3OH)\cdot CO_3^{2-}]$: C, 35.54%; H, 5.66%. Found: C, 36.00%; H, 5.73%.

2.2.1.4. β-CD-K (Compound 4). β-CD (130 mg, 0.11 mmol) and KOH (51 mg, 0.9 mmol) were dissolved in H_2O (3.25 mL). The solution was filtered through a *m* syringe filter and decanted into separate vials. Add THF (0.33 mL). MeOH or THF (5 mL) was allowed to diffuse slowly into the solution over a period of a week. Colorless cubic crystals suitable for X-ray crystallographic analysis were isolated, filtered, and washed with MeOH (3 × 5 mL) (yield: 55–65%). $[2(C_{42}H_{70}O_{35})\cdot 2K^+\cdot17(H_2O)\cdot CO_3^{2-}]$: C, 37.17%; H, 6.46%. Found: C, 37.15%; H, 6.25%.

2.2.2. Solvent Exchange Method. 2.2.2.1. β-CD-K (Compound 4). The synthetic protocol for CD MOF was adopted from the reported procedures β-CD-K,[18] and different solvents were then added to the MOF to exchange the solvent in structure.[26]

2.2.3. Fast Crystallization. Method protocol—the synthetic protocol for CD MOF was adopted from the standard procedure.[8] The difference is in the process when a second solvent, which promotes crystal formation and crystallization,

is added. The solvent is not diffusing into a water solution for some time in this method, but all of the solvent is added to the reaction mixture to ensure immediate precipitation.

2.2.3.1. γ-CD-K-1 (Compound 5). γ-CD (648 mg, 0.5 mmol) and KOH (448 mg, 8 mmol) were dissolved in H_2O (10 mL). The obtained solution was stirred for 30 min at RT. MeOH (12 mL) was added to the water solution. The precipitate was filtered and washed with MeOH. The obtained precipitate was dried at RT (21–25 °C) (yield: 80–90%). Elemental analysis (%) calculated for $[C_{48}H_{80}O_{40}\cdot2K^+\cdot16-(H_2O)\cdot2OH^-]$: C, 33.96%; H, 6.65%. Found: C, 34.01%; H, 6.10%.

2.2.3.2. γ-CD-K-2 (Compound 6). γ-CD (648 mg, 0.5 mmol) and KI (1328 mg, 8 mmol) were dissolved in H_2O (10 mL). The obtained solution was stirred for 30 min at RT. MeOH (30–50 mL) was added to the water solution until precipitation began. The precipitate was filtered and washed with MeOH for a short time. The obtained precipitate was dried at RT (21–25 °C) (yield: 70–80%). $[C_{48}H_{80}O_{40}\cdot2K^+\cdot10(H_2O)\cdot1.8OH^-\cdot0.2I^-]$: C, 35.78%; H, 6.25%. Found: C, 36.03%; H, 5.84%.

Single crystals of compound **6** were obtained as follows: γ-CD (648 mg, 0.5 mmol) and KI (1328 mg, 8 mmol) were dissolved in H_2O (10 mL). The obtained solution was stirred for 30 min at RT. Add MeOH (12 mL). Leave the vial closed until crystals are formed (appx. 24 h).

2.3. Characterization of the Newly Obtained CD MOFs. *2.3.1. X-ray Diffraction Methods.* Powder X-ray diffraction (PXRD) patterns were measured at ambient temperature on a D8 Advance (Bruker) diffractometer using copper radiation (Cu Kα) at a wavelength of 1.54180 Å, equipped with a LynxEye position-sensitive detector. The tube voltage and current were set to 40 kV and 40 mA. The divergence slit was set at 0.6 mm, and the anti-scatter slit was set at 8.0 mm. The diffraction patterns were recorded using a 0.2 s/0.02° scanning speed from 3 to 35° on a 2Θ scale.
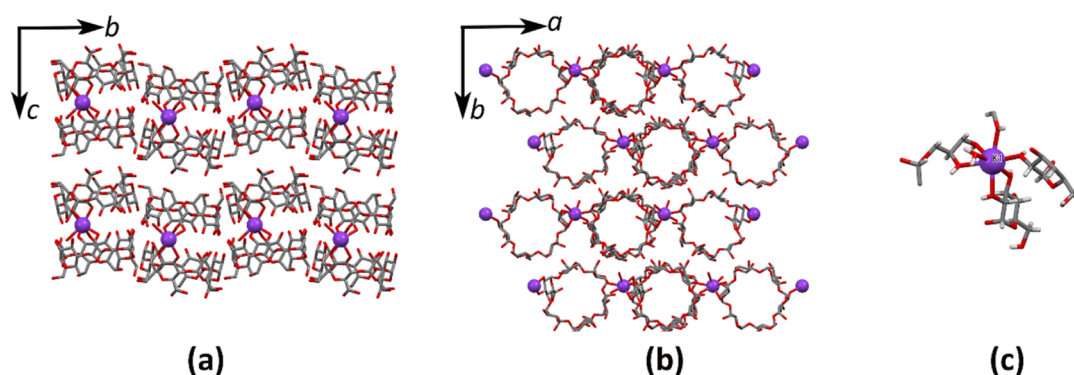
Figure 1. (a,b)—molecular packing and (c)—coordination of the K$^+$ ion of compound **1**.

Variable-temperature (VT) PXRD patterns were measured on a D8 Discover (Bruker) diffractometer equipped with a MRI temperature chamber. The diffraction patterns were recorded using a 0.5 s/0.02° scanning speed from 3 to 30° on a 2Θ scale. Other settings and equipment were identical to those used for the D8 Advance instrument mentioned earlier.

Single-crystal X-ray diffraction (SCXD) studies were performed on an XtaLAB Synergy-S Dualflex diffractometer (Rigaku Oxford Diffraction) equipped with a HyPix6000 detector and a microfocus sealed X-ray tube with Cu Kα radiation (λ = 1.54184 Å). During data collection, the crystals were maintained at 150 K.

We conducted synchrotron SCXD studies on compound **6**. Diffraction data were collected at beamline P24 of PETRA-III at the German Electron Synchrotron (DESY) facility. A wavelength of 0.5000 Å was used. The data were recorded on a Pilatus 1 M CdTe detector. 3600 frames were collected with an exposure time of 1 s per 1°. Each consecutive 10 frames were subsequently binned using the Pilatus software[27] to obtain 360 frames of 1° per frame. Datasets were collected at 150 K using an open-flow nitrogen cryostat CRYOCOOL.

The structure was solved using direct methods with the ShelXT program using intrinsic phasing[28] and refined using full-matrix least-squares techniques on F^2 with the SHELXL[29] package.

Graphics of the crystal structures were drawn, and the solvent-accessible volumes and the volume of the cavities were calculated using Mercury software.[30] The resolution was 0.2 distance/Å, and the probe grid was 0.5 Å. To determine the true cavity volume, all solvent molecules in the structure were deleted before calculation. The packing index was calculated using PLATON[31] software.

Crystallographic data and structure refinement details for compounds **1** (α-CD-K-1), **2** (α-CD-K-2), **3** (α-CD-Rb-1), **4** (β-CD-K-1), and **6** (γ-CD-K-1) are presented in Table 2. The full dataset is available in the form of CIF files deposited with the CCDC (2236391−2236393, 2236395, and 2236396) and may be obtained free of charge via https://www.ccdc.cam.ac.uk/structures. Full crystal data and structural refinement details for compounds **1**, **2**, **3**, **4**, and **6** are available in Table S1.

The simulated and experimental compound PXRD pattern comparison can be seen in the Supporting Information in Section S2 and Figures S1−S4.

2.3.2. Thermal Stability and Activation. To reduce the amount of solvent in the synthesized sample, the vacuum method for sample activation was selected because this process has been widely used for MOF activation.[32] Because the synthesized samples already contained a low-boiling point solvent−methanol, the solvent exchange process was not performed. The sample was evacuated (10^{-3} Torr) at RT for 10 h.

Differential scanning calorimetry/thermogravimetric (DSC/TG) analyses were performed on a TGA/DSC2 apparatus (Mettler Toledo) using open 100 L aluminum pans. Samples with a mass of 3−10 mg were heated under a nitrogen atmosphere (flow rate 100 ± 10 mL·min^{-1}) at a temperature range of 25−450 °C (heating rate 10°·min^{-1}).

2.3.3. Calculation of the Intermolecular Interaction Using Hirshfeld Surface Analysis. To quantitatively compare the different intermolecular interactions affecting the molecular packing in the compound under study, a Hirshfeld surface analysis was employed. The strength of the present intermolecular interactions can be displayed on the Hirshfeld surface.[33] The crystallographic information file (.cif) is given as input to the Crystal Explorer program. The Hirshfeld surface is unique for a given crystal structure and a set of atomic electron densities. Each point on the Hirshfeld surface is specified with two distances: d_i is the distance from the Hirshfeld surface to the nearest nucleus inside the surface and d_e is the distance from the nearest nucleus outside the surface. Then d_{norm} is the normalized contact distance, which is defined in terms of d_i, d_e, and the van der Waals radii (vdW) of the atoms.

2.3.4. N$_2$ Adsorption−Desorption Measurements. The activated samples were used for sorption measurements. The surface area of the samples was determined using a nitrogen adsorption−desorption isotherm at 77 K with the Nova 1200 nitrogen adsorption instrument (*Quantachrome*). Surface area determination was performed using methodology from the literature.[34]

2.3.5. Evaluation of Stability in Various Solvents. To evaluate the stability of the newly obtained compounds in various solvents, we immersed the bulk powder of CD MOFs in toluene, methanol, THF, and isopropanol for 2 weeks for each solvent. During the stability experiment, the respective solvents were exchanged every day.[26] Every 3 days, samples were analyzed by PXRD.

3. RESULTS AND DISCUSSION

As a result of the conducted research, we obtained and characterized six new CD (α-, β-, and γ-CD)-based MOFs with K$^+$ and Rb$^+$ cations. Five MOFs were structurally characterized by a SCXD, and one was characterized as a bulk powder. Compound **5** was characterized by inductively coupled plasma mass spectrometry (ICP−MS) to confirm the potassium ion and its amount in the structure. Compound **1** repeat

crystallization failed (short analyses of the failed attempt can be seen in Section S3).

3.1. Structure Description. The SCXD analyses reveal that compounds **2** and **3** are isostructural and form a 3D framework, while compound **1** possesses the same space group and framework (2D) type as EVEGET (α-CD-K), as stated in the published literature.[20] Compound **1** crystallizes in the monoclinic crystal system with the $P2_1$ space group. Compounds **2** and **3** crystallize orthorhombic crystal systems with the $P2_12_12_1$ space group and are more densely packed than compound **1** and EVEGET (α-CD-K) and MAMVED (α-CD-Rb).[25]

In the asymmetric unit, compound **1** consists of two CD and one potassium ion and disordered water/methanol molecules (therefore, the SQUEEZE procedure was performed). EVEGET in the asymmetric unit consists of two CD molecules, three potassium molecules, and seven water molecules. In compound **1**, the potassium coordination number is 7 (see Figure 1c). Potassium forms coordination to four separate α-CD tori with glycosidic ring hydroxyl groups from the secondary face. The longest K−O bond length is 2.774 Å and the shortest is −2.692 Å. Two coordination bonds are formed with adjacent glycosidic ring hydroxyl groups from one CD moiety. The amount of solvent molecules in the final structure depends on the degree of disorder in the structure and how easily it can be detected and fixed in the position. To decrease R % for the structure, we lost information about solvent molecules in the crystal lattice.

Since compounds **2** and **3** are isostructural here, take compound **2**, for example, their structures are described in detail. The asymmetric unit consists of one CD, two potassium, one methanol, and five water molecules (the detected solvent molecule amount can change in the structure depending on the degree of disorder). There are two types of K$^+$ ions in compound **2** [see Figure 2B(a,b)]. The coordination number of one potassium ion is 7 and the other is 8—K(1) and K(2), respectively. K(1) bonds with one water molecule (2.927), one carbonate ion (2.918), and three
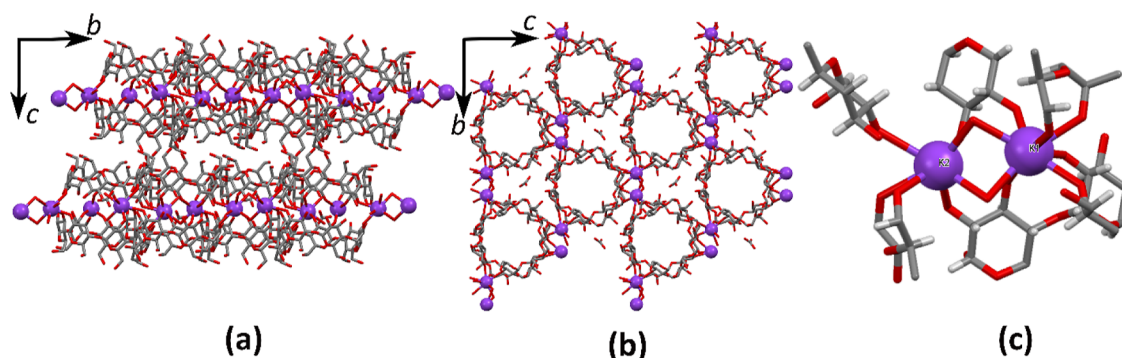

Figure 2. (A)—Molecular packing of compound **2**. Black and blue lines are added for the CD moiety arrangement clarity in the lattice. Hydrogen atoms have been omitted for clarity. (B)—Coordination of (a) K(1)$^+$ and (b) K(2)$^+$ ions of compound **2**.

separate α-CD tori with glycosidic ring hydroxyl groups. One hydroxyl group belongs to the primary face, and another three are from the secondary face. Two coordination bonds are formed with two hydroxyl groups from one CD moiety. The longest K−O bond length is 3.300 and the shortest is −2.640 Å. One coordination is formed with the glycosidic ring oxygen atoms instead of the hydroxyl group, and the K−O bond length is 2.964 Å. K(2) coordinates with two water molecules, and the K−O bond lengths are 2.847 and 2.875 and to four separate α-CD tori with glycosidic ring hydroxyl groups. Two coordination bonds are formed with two hydroxyl groups from one CD moiety. The two hydroxyl groups are from the primary face and another four are from the secondary face. The longest K−O bond length is 3.385 Å and the shortest is 2.769 Å. K(1) forms a coordination bond stronger than K(2).

In compound **2**, the remaining α-CD and potassium moieties are arranged in zigzag chains and do not form channels (see Figure 2A). Adjacent α-CD moieties are located in opposition down the crystallographic b-axis. Compound **1**: the remaining α-CD moieties are arranged in layers (see Figure 1a) and two α-CD tori are fused together tail to tail themselves (down the crystallographic a axis). A similar arrangement can be observed in the EVEGET structure. In both structures, K ions connect those two α-CD molecules together. The 2D sheets are aligned offset with the primary faces of the α-CD tori facing each other, although they are not coordinated by any K$^+$ ions. The difference between compound **1** and EVEGET is in the channel type and potassium amount in the structure. The compound **1** channel is straight (view down the crystallographic c axes), but in EVEGET (view down the crystallographic b axis), layers are shifted with respect to each other and do not form a straight channel. That channel type would be a problem for larger molecules to incorporate into the structure, despite the void-accessible volume size.

Compound **4** crystallizes in the monoclinic crystal system with the $P2_1$ space group. It has the same space group and framework (2D) type as KOBRIC/PULLOF (β-CD-K) in the published literature,[17] but the molecule arrangement is completely different. It is more similar to compound **1** and EVEGET. Compound **4**: the remaining β-CD moieties are arranged in layers and two β-CD tori are fused tail to tail (view down the crystallographic b axis). The potassium ions join those two β-CD molecules together (Figure 3c). CD rings form a channel along the a axis, like in compound **1**. In the KOBRIC/PULLOF structure, β-CD rings do not form a channel. The asymmetric unit consists of two CDs, two potassium ions, and one carbonate ion. One potassium's coordination number is 8 and the other is 7—K(1) and K(2), respectively. The compound **4** K(1) atom coordinates with two oxygen atoms (2.819 and 2.870) to form four separate β-CD tori with glycosidic ring hydroxyl groups from the secondary face. The longest K−O bond length is 2.967 Å and the shortest is −2.782 Å. K(2) forms coordination with two oxygen atoms (2.807 and 2.884 Å). The oxygen atom forms coordination with both potassium atoms (Figure 3c). Such coordination has not been observed in other structures. These oxygen atoms are associated with one hydrogen atom and most likely they are hydroxide counterions that are incorporated during crystal formation. There were no density clouds for another hydrogen atom around the oxygen atom in the structure refinement process; thus, we think that these are hydroxide counterions. Similar to K(1), K(2) coordinated to four separate β-CD tori with glycosidic ring hydroxyl groups
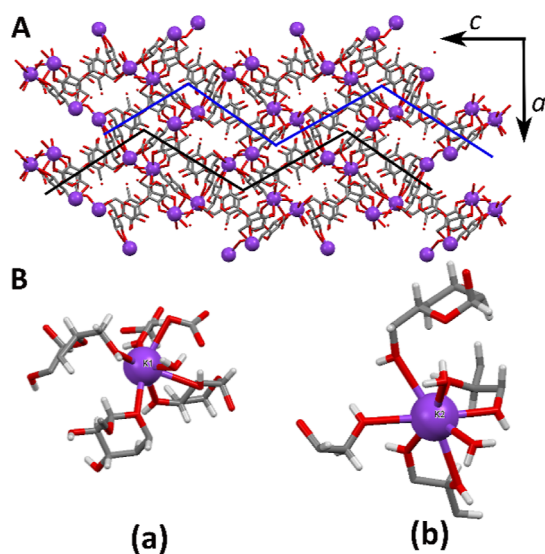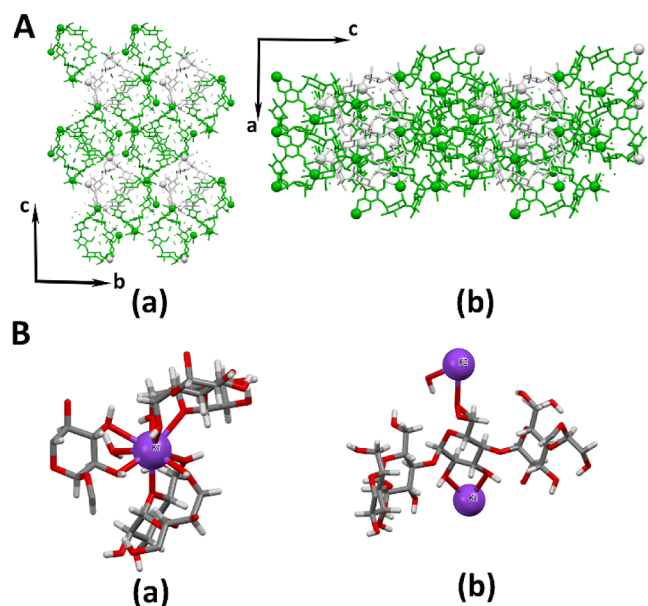
Figure 3. (a,b)—Molecular packing and (c)—coordination of the K$^+$ ions of compound **4**.

from the secondary face. The longest K−O bond length is 3.080 Å and the shortest is −2.749 Å. The carbonate ion does not form coordination with metal ions, as in compounds **2** and **3**.

Compound **6** crystallizes in the orthorhombic crystal system with the $P2_12_12_1$ space group and forms a 2D framework type. The compound **6** structure is the same as that of TOHXIA[22] as stated in the published literature, but the main difference is the amount of potassium in the structure. There is one potassium atom in the asymmetrical unit with coordination number 8 in TOHXIA, but our presented structure has two potassium atoms in the asymmetrical unit. The measured crystal of compound **6** has large disorder factors from solvent molecules.

Compound **6** and the remaining γ-CD are arranged in step-type layers (see Figures 4 and 5) and do not form channels.

Figure 4. (A)—Molecular packing of compound **6**. Hydrogen atoms are omitted for clarity. (B)—Coordination of (a) K(1)$^+$ and (b) K(2)$^+$ ions of compound **6**.

The one-layered CD moieties are arranged in one direction along the *a* axe, but if we put together two-layered CD moieties, they are in opposition to each other. Therefore, two-layered (along the *a* axe) CD moieties are perpendicular to each other (see Figure 5c). The asymmetric unit consists of one CD, two potassium ions, one iodine ion with occupancy 0.2, one methanol molecule, two water molecules, and three

water molecules with occupancy 0.5. There are 3 hydroxyl groups with occupancy 0.5 and 0.8 in one case in the asymmetrical unit. The inferior occupancy shows that the structure is disordered. One potassium coordination number is 9 and the other is 2—K(1) and K(2), respectively. The coordination number 2 of potassium in MOFs was not observed before. In compound **6** K(1), it coordinates with one water molecule with a bond length of 3.039 and to 8 oxygen atoms. The two coordinations are with hydroxyl group oxygen atoms from the same glycosidic ring (2.705 and 2.874 Å) from the secondary face. Another six coordinations are with two different γ-CD rings of oxygen atoms from the primary face. The four coordinations are with hydroxyl group oxygen atoms and two are with glycosidic ring oxygen atoms. The K(2) coordinates with the water molecule (2.50 Å) and primary face hydroxyl group oxygen atom (3.10 Å).

Hirshfeld surface analysis was carried out to get a better comprehension on the nature of the packing motifs and the contribution of the main intermolecular interactions directing the molecular architecture in compounds **1**−**6** (except **5**). The relative contributions to the Hirshfeld surface area due to the main intermolecular interactions are shown as a histogram in Figure 6.

It was found from the 2D FP plot analysis that the H···H bonds are dominant and cover the total HS area in the range of 48% in compound **6** to 57% in compound **4**. On the other hand, subtle interactions such as H···O/···H are also significant contributors, associating from 34% in compounds **2** and **4** to 40% in compound **6**%, providing extra stabilization in addition to the presence of the strong hydrogen bonds above. Besides, H···X$^+$ (where X$^+$ means alkali metal cations) contacts seem also important from 1% for compound **3** to 4% in compound **6**. O···X$^+$ contacts from 3% in compound **1** to 3% in compound **3** are at a similar level. The interaction between the oxidized O···X$^+$ complex and the—H···X$^+$ complex is stronger. Although compounds **2** and **3** are isostructural, some intermolecular contacts are different. H···H bonds are more dominant in compound **2** than in compound **3**, in which the H···O/O···H dominate more. Most probably, it relates to the different solvent content on the measured crystal.

As can be seen from Figure 7, both compound Hirshfeld surface analyses are practically the same because of the identity of the main structures of both compounds. The main difference is in the H/O···K$^+$ interaction—compound **6** has two potassium in the asymmetrical unit. Also, a wider area from the H···O and H···H interactions in compound **6** is observed; we were able to determine the solvent molecule and present it in the structure.

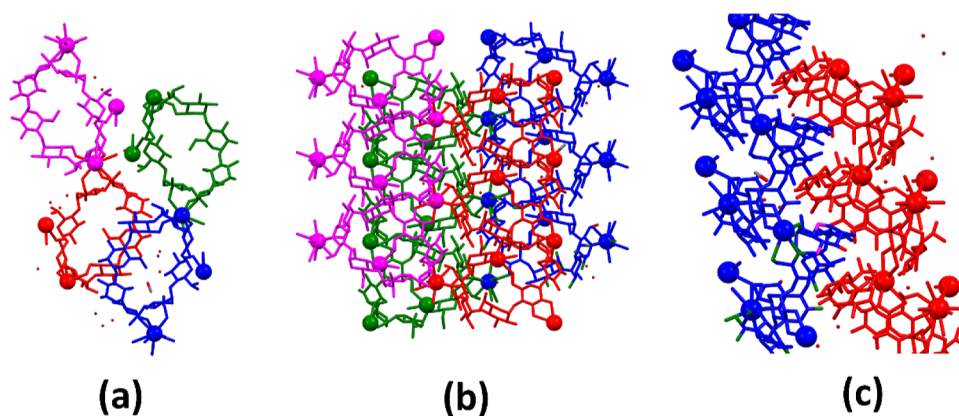**Figure 5.** Molecular packing of compound **6**: (a)—view down the *a* axe; (b)—view down the *b* axe; and (c)—along the *a* axe.
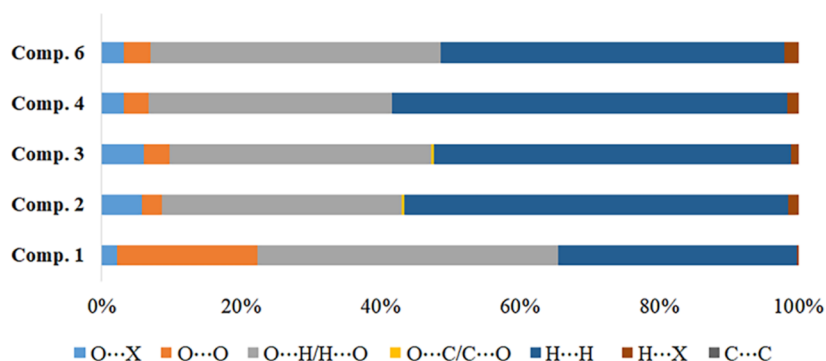

Figure 6. Relative contributions of the main intermolecular contacts with the Hirshfeld surface area in compounds **1**−**6** (except **5**). X is the corresponding metal ion in the structure.
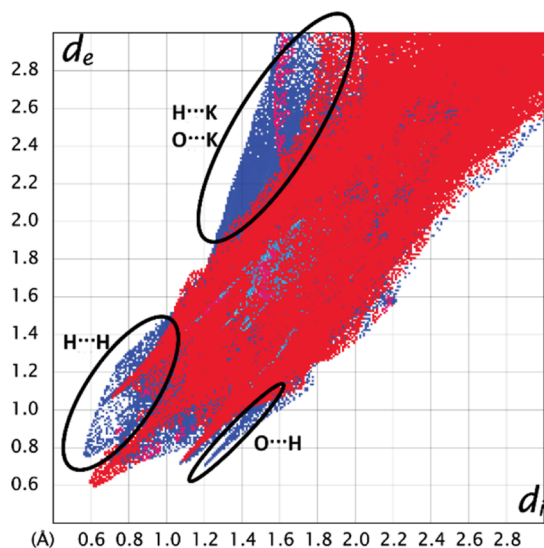

Figure 7. Overlaying Hirshfeld surface analysis of compound **6** and TOHXIA. Blue is for compound **6** and red is for TOHXIA.

3.2. Design and Synthesis. In this research, we adopted a method from the standard procedure and investigated the possibility of whether the fast crystallization principle provides the same crystal phases as the classical procedure—vapor diffusion crystallization. The synthesis of the MOF requires: (a) the addition of the necessary amount of solvent to the aqueous reaction mixture for solid formation until all the solids are crystallized out—no solvent diffusion into the water

solution; (b) the hydroxide substance mole ratio is two times bigger (16 equiv) than in the standard procedure, but for other substances it remains the same (8 equiv); and (c)—an immediate solid filtration after formation and washing with a solvent used for crystallization to remove unreacted metal compounds. The obtained results are summarized in Table 3.

Table 3 shows the experimental conditions and solvents used (solid powder patterns for all of the experiments are available in Section S5 from Figures S6−S14). As can be seen in Table 3 results, in α-CD cases with potassium hydroxide crystallized out of EVEGET with low crystallinity but a reaction with potassium carbonate, it is possibly getting the same phase-compound **2**—what we obtained in the classical crystallization method and for the first time described crystal structure in this publication above. As can be seen in Table 3, α-CD crystallized out as EVEGET with potassium hydroxide. However, the crystallinity was low. The reaction with potassium carbonate gives the possibility of getting the same phases (compound **2**) that we obtained with the classical crystallization method and whose crystal structure was described for the first time in the publication above. The drying of the precipitate does not affect the selected solid phase. We also obtained the same phases as in the classical crystallization with rubidium hydroxide (compound **3**), but this time we used more than 10 mL of solvent to precipitate the solid. The reaction with CsOH gave a very similar pattern to YAPRUE (γ-CD-Cs) with α-CD impurity. Repeating crystallization several times did not give any crystalline material. Therefore, we could not draw a conclusion from the crystallization results. The reaction with sodium hydroxide

Table 3. Obtained Crystallization Results Using the Modified Vapor Diffusion Method[a]

	T, °C	α-CD (1 equiv)	β-CD (1 equiv)	γ-CD (1 equiv)
KOH (16 equiv)/MeOH	25	LC EVEGET	LC β-CD-K	comp. 5
	80	LC EVEGET	A	A
KOH (8 equiv)/MeOH	25	LC EVEGET	LC β-CD-K	A
	80	LC EVEGET	A	A
KOH (16 equiv)/EtOH	25	LC EVEGET	β-CD-EtOH	LC γ-CD-K-α
	80	LC EVEGET	A	γ-CD-K-α
KOH (8 equiv)/EtOH	25	comp. 2 + extra peak	A + LC β-CD-K	A
	80	comp. 2 + extra peak	A + LC β-CD-K	γ-CD-K-α
K₂CO₃ (8 equiv)/MeOH	25	comp. 2	β-CD-K	comp. 5
	80	comp. 2		γ-CD-K-δ
K₂CO₃ (8 equiv)/EtOH	25	comp. 2	K₂CO₃	K₂CO₃
	80	comp. 2	A	K₂CO₃
NaOH (16 equiv)/MeOH	25	A	A	LC γ-CD-Na
	80	A	A	γ-CD-Na
NaOH (8 equiv)/MeOH	25	A	Na₂CO₃	Na₂CO₃
	80	A		A
NaOH (16 equiv)/MeOH	25	A	β-CD	γ-CD + γ-CD-Na
	80	A	β-CD	A + Na₂CO₃
NaOH (8 equiv)/EtOH	25	A	LC UK	γ-CD-Na
	80	A	LC UK	γ-CD-K–Na

	α-CD (1 equiv)	β-CD (1 equiv)	γ-CD (1 equiv)
Na₂CO₃ (8 equiv)/MeOH	Na₂CO₃	β-CD	Na₂CO₃
Na₂CO₃ (8 equiv)/EtOH	Na₂CO₃	β-CD	Na₂CO₃
		Na₂CO₃	γ-CD-K–Na + Na₂CO₃
RbOH (16 equiv)/MeOH	comp. 3[b]	β-CD	γ-CD-Rb + γ-CD·MeOH·H₂O
CsOH (16 equiv)/MeOH	UK/A	β-CD	γ-CD-Cs + extra peak
KF (8 equiv)/MeOH	no solid	no solid	A[b]
KBr (8 equiv)/MeOH	no solid	no solid	A[b]
KI (8 equiv)/MeOH	no solid	no solid	γ-CD-K-α/γ-CD-K-2[b]

[a]T—precipitates drying temperature (±2 °C); A—amorphous; UK—unknown compound; and LC—low crystallinity of the sample. [b]More solvent is used for precipitation, as stated in the methodology description.
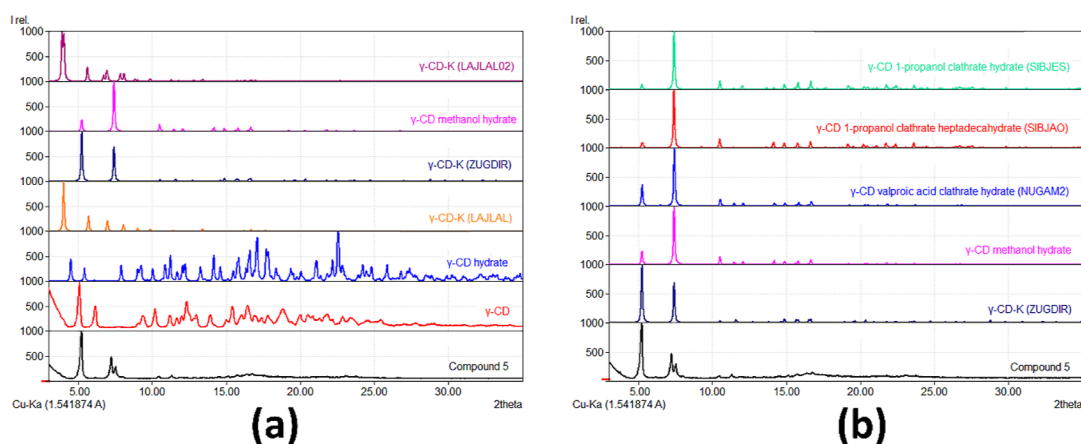
Figure 8. (a)—Compound **5** pattern compared to other γ-CD compound patterns and (b)—the compound **5** pattern compared to other similar γ-CD compound patterns.
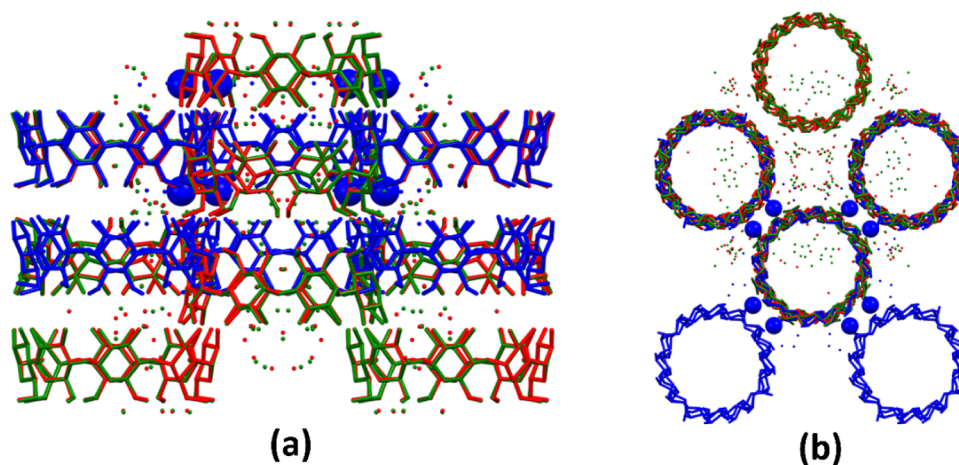
Figure 9. Overlay structures for SIBJAO (red), NUNRIX (green), and ZUGDIR (blue): (a)—view down direction *a* and (b)—view down direction *c*. Hydrogen atom is omitted for clarity.

gave amorphous material, but potassium halides did not have any solid.

Already known phases crystallized in the β-CD-KOBRIC/PULLOF with KOH and K_2CO_3; either the crystallinity was low or we obtained a mixture with an amorphous phase. The reaction with NaOH, Na_2CO_3, and RbOH/CsOH did not give any MOF. It could be connected to low β-CD solubility in water. The reactivity of potassium halides was also checked, but such compounds did not give any solids like α-CD.

As can be seen in Table 3, γ-CD cases reaction results of the obtained γ-CD-K phases involved precipitate drying temperature and used solvents in the crystallization process (we presented only two solvents in the publication—there was no precipitation with other solvents). We therefore think that thermodynamic and kinetic factors are involved in the phase formation process: fast crystallization should form a kinetic product and slow crystallization should form a thermodynamic product, γ-CD-K α phase. We also obtained the γ-CD-K α phase in the drying process using elevated temperatures. Products formed in the reaction with potassium carbonate gave the γ-CD-K (ZUGDIR) phase after the drying process (obtaining the product in a solvent exchange process, whose characterization was described in our previous research).[16] The reaction with NaOH gave already known phases, YAPROY. γ-CD methanol hydrate (NUNRIX) crystallized together with a

small amount of LAJLEP in the reaction with RbOH. CsOH also gave a mixture of γ-CD methanol hydrate (NUNRIX) and γ-CD-Cs (YAPRUE). One extra unidentified peak was also observed. New phases were formed in the crystallization with potassium hydroxide. The new phase's PXRD pattern is shown in Figure 8. It is compared to other known γ-CD compound PXRD patterns.

As shown in Figure 8a, the compound **5** pattern is very similar to γ-CD methanol hydrate (NUNRIX) and γ-CD-K δ phase patterns (we got these phases in the drying process), but there are two peaks in region 7−8° 2θ scale for the compound **5**—that way we think that it is another γ-CD-K phase. We cannot obtain a suitable crystal for SCXRD analysis by using this crystallization protocol (the crystal diffraction is very weak). This type of phase formation has not been observed in other obtaining methods. We analyzed the amount of potassium in the sample with the ICP−MS method (see Section S4 for details on sample preparation and measurements). It is shown that the sample contains potassium, and we can assume that it is a MOF—the analyses detected 3% potassium in the sample, which is an approximate ratio for one potassium ion to one γ-CD molecule (excluding solvent molecules). We compared the compound **5** pattern to the already published γ-CD compound pattern (similar PXRD

patterns) and analyzed the construction of the possible structure.

As shown in Figure 8b, the compound **5** pattern is very similar to the powder patterns of other γ-CD compounds' powder patterns. Therefore, we think that compound **5** structure could be very similar to those compounds' molecule arrangements because it is identical to the structure arrangement in the γ-CD moiety (see Figure 9). The cell parameters and space groups are different: $P42_12$ (SIBJES, SIBJAO,[35] and NUNRIX)[36] and $I4$ (ZUGDIR).[16] As can be seen from Figure 9, the γ-CD rings' arrangement is practically the same in downward view *c* and slightly shifted (ZUGDIR cases) in one line in the view down direction *a*. Only the metal ions are located between these rings, which does not affect the pattern.

If it is known from the literature[37] whether the two phases have similar structures, we can examine the relation between those two phases. If peak splitting is observed in the pattern, then a phase transition is possible. The 200 peak splits into two peaks (many cases of approximately equal intensity), which have an index of −200 and 002. This type of peak splitting would correspond to a tetragonal to orthorhombic phase transition. However, if the 211 reflection is observed and if it splits into three peaks, then the second phase is likely to be in the monoclinic system. Because of the low crystallinity of compound **5**, it is not possible to correctly make a conclusion about peak splitting on the larger angle in the 2θ scale. We can assume that the phases are very similar to each other, and there should be involved second-phase transitions. The phase transition should occur from tetragonal $I4$ to orthorhombic or monoclinic crystal systems. We measured a PXRD pattern for compound **5** in situ from 25 to 205 °C to confirm this theory.

As can be seen from the obtained results (Figure 10), a change of compound **5** patterns occurred (in all temperatures
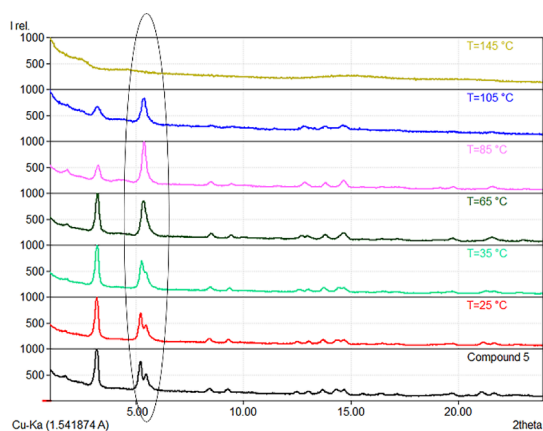
Figure 10. In situ XRD patterns of compound **5** upon increasing temperature (measurement step, 10 °C).

recorded, PXRD can be seen in Figure S14.) at elevated temperature. The peaks between 7 and 8° on 2θ scale are changing and they are merging during heating process—they merge completely in temperatures above 50 °C. The amorphous phase is formed in temperatures above 130 °C.

Only one peak is observed at an elevated temperature. The obtained results confirm the previously made statement: if phase transition is involved, higher symmetry would appear in the case of a solid with similar structure at elevated

temperature. Therefore, compound **5** should crystallize in a lower symmetry than the ZUGDIR phases.

To evaluate the thermal and architectural stabilities of the new crystal phases of CD MOFs, we examined their thermal stabilities using DSC/TG analysis. The activated sample was measured and compared with that of activated γ-CD-K-α (LAJLAL).

The thermal stability results are summarized in Figure 11. We compared the results to γ-CD-K α phase DSC/TG values. As shown in Figure 11, the DSC and TGA curves of all of the analyzed phases have similar patterns. The weight loss can be divided into two parts: (1) the loss of the solvent that is inside the pore and/or absorbs on the surface and (2) the decomposition of the MOF itself. First, weight loss of increasing temperature is observed (the onset temperature of the first peak is $T_\alpha = 34$, $T_6 = 36$ °C, $T_5 = 41$ °C, $T_4 = 69$ °C, $T_3 = 88$ °C, and $T_2 = 88$ °C), and it can be primarily associated with the loss of solvent molecules residing in pores; it was in the range 9−13% in the sample. A possible higher onset temperature relates to dense packing of the structure and difficulties for the solvent to escape from the structure. Experimental data indicate that the newly obtained phases of CD MOF are thermally stable up to 250 °C. Compound **4** is an exception, as it decomposes at a higher temperature (310 °C). A partial decomposition of the ligand occurs at a higher temperature. The weight loss for all crystal phases is in the range of 45 to 65% and it is related to the elimination of hydroxyl groups present in the CD unit and further destruction of glucose units. Furthermore, DSC results show a possible phase transition in compound **2** with an endothermic effect peak at $T_{onset} = 168$ °C and in compound **6** with an endothermic effect peak at $T_{onset} = 237$ °C just before decomposition occurs.

We compared the TG trace of as-synthesized and activated samples of all compounds (see Section S7 in Figure S15). The obtained data lead to the inference that the activation process diminishes the presence of solvent molecules within the compound's structure and slightly increases its thermal stability.

Nitrogen gas adsorption−desorption was used to measure the porosity of the newly obtained compounds. For the measurements, an activated sample was used. The obtained isotherms are shown in Section S8 and Figure S16. The isotherms of all newly obtained MOFs show type III. Type III isotherm is very rare; therefore, we applied the BET equation to find out the *c* constant. To be sure that it is a type II isotherm without a knee. Because sometimes, if there is not enough data, it does not show the knee. All calculated *c* constant (see Section S8) values were larger than 2, which means that all obtained isotherm is II not III. Different from LAJLAL, which has a first-type isotherm.[8] The isotherm can be divided into two parts: (1) during the first part of the isotherm, the nitrogen gas uptake slowly increased, indicating that the adsorption mechanism had been transmitted from the single-molecule adsorption to multilayered adsorption in the MOFs and (2) in the second part of the isotherm, the gas uptake increased slightly faster. That indicates that capillary condensation occurred.[38] Gas uptake increased in the following order: compounds **2**, **6**, **3**, **4**, and **5**. The calculated BET surface area was 692 m^2/g for LAJLAL (synthesized according to the literature protocol),[8] which was smaller than that reported previously.[8] This can be explained by the solvent molecules located in the sample's MOF pores. That means that
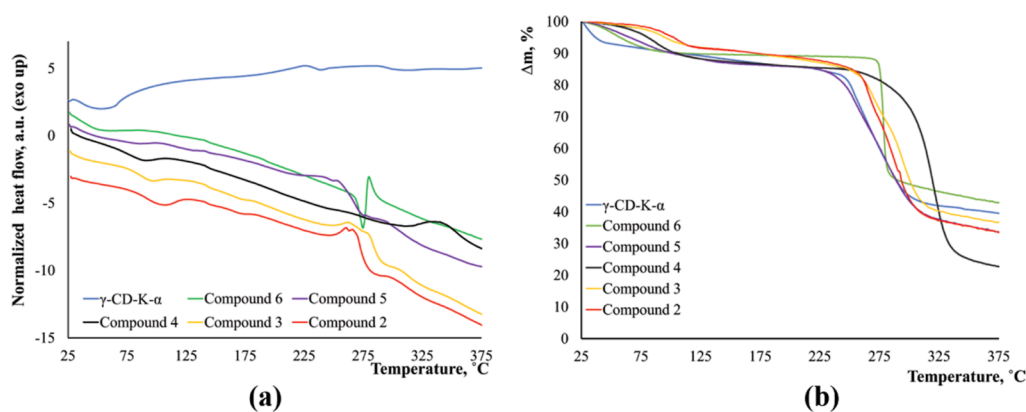
Figure 11. (a) DSC and (b) TGA curves of newly obtained CD MOFs (except compound **1**).

the sample activation was partial. The calculated apparent surface area for compound **5** is 324 m^2/g, compound **4**—139 m^2/g, compound **3**—12 m^2/g, compound **6**—6 m^2/g, and compound **2**—3 m^2/g. The obtained results agree with the calculated solvent accessible volume (Table 2). The hysteresis for all data was observed, which indicates the presence of porous surfaces.

To evaluate the stability of the newly obtained compounds, the bulk powder was immersed in various solvents (methanol, toluol, isopropanol, and THF), and the PXRD patterns were recorded before, during, and after the experiments. The obtained results are shown in Table S2. From the obtained results, it can be concluded that in almost all tested solvents, newly obtained CD MOFs are stable, and only in THF compounds **2**, **3**, and **5** decreased crystallinities (detected by PXRD), whereas compound **6** was stable only in methanol in another solvent that it decomposed. This can be explained by structural instability because the second potassium coordination is the only one that can promote molecule rearrangement in the solvent.

4. CONCLUSIONS

In summary, six new CD MOFs were synthesized, and their unique structures were studied. Two of the structures are isostructural compounds **2** (α-CD-K-2) and **3** (α-CD-Rb-3). The isostructurality between CD-based MOFs is not rare. Compound **1** (α-CD-K-1) was characterized by SCXRD, and repeated crystallization of the single crystals failed. Compounds **1** (α-CD-K-1) and **4** structure architectures are similar but different in CD ring type. Compound **5** was characterized by PXRD and ICP−MS, and the results suggest that it is γ-CD-K with an orthorhombic or monoclinic structure. The phase transition occurs from compound **5** to the higher symmetry compound γ-CD-K δ, and the second phase transition occurs at elevated temperatures.

Compound **6** crystallized on an orthorhombic crystal system, and the main crystal pattern was the same as that of TOHXIA. The main difference is the amount of potassium in the structure. Our method for obtaining compound **6** is faster and easier than that reported in the literature.

For the first time, modified vapor diffusion methods were successfully used to obtain the MOF. These methods promote fast results, and it is possible to simultaneously obtain a larger amount of the compound. The disadvantage of this method is the use of a larger amount of solvent. By changing the type of solvent and the drying temperature of the precipitates, it is

possible to obtain different phases in a controlled manner. This method allowed us to obtain compound **5** for the first time. Other methods for obtaining this compound are unknown.

■ ASSOCIATED CONTENT

ⓢ Supporting Information

The Supporting Information is available free of charge at https://pubs.acs.org/doi/10.1021/acsomega.3c07429.

> Crystallographic data and lattice parameters, simulated and experimental PXRD patterns, PXRD pattern of compound 1 failed crystallization experiments, ICP−MS method sample preparation and experimental condition, solid powder patterns collected from all fast crystallization experiments, XRD patterns collected at elevated temperature in situ, TG traces for an as-synthesized and an activated samples, N$_2$ adsorption−desorption measurements, and evaluation of stability in various solvents (PDF)

■ AUTHOR INFORMATION

Corresponding Author

> **Kristīne Krūkle-Bērziņa** − *Latvian Institute of Organic Synthesis, Riga LV-1006, Latvia;* ⓘ orcid.org/0000-0003-0899-3927; Email: kkberzina@osi.lv

Author

> **Anatoly Mishnev** − *Latvian Institute of Organic Synthesis, Riga LV-1006, Latvia*

Complete contact information is available at:
https://pubs.acs.org/10.1021/acsomega.3c07429

■ REFERENCES

(1) Roy, I.; Stoddart, J. F. Cyclodextrin Metal−Organic Frameworks and Their Applications. *Acc. Chem. Res.* **2021**, *54*, 1440.

(2) Nadar, S. S.; Vaidya, L.; Maurya, S.; Rathod, V. K. Polysaccharide Based Metal Organic Frameworks (Polysaccharide-MOF): A Review. *Coord. Chem. Rev.* **2019**, *396*, 1−21.

(3) Domingos, S.; André, V.; Quaresma, S.; Martins, I. C. B.; Minas da Piedade, M. F.; Duarte, M. T. New Forms of Old Drugs: Improving without Changing. *J. Pharm. Pharmacol.* **2015**, *67* (6), 830−846.

(4) Rajkumar, T.; Kukkar, D.; Kim, K. H.; Sohn, J. R.; Deep, A. Cyclodextrin-Metal-Organic Framework (CD-MOF): From Synthesis to Applications. *J. Ind. Eng. Chem.* **2019**, *72*, 50−66.

(5) Han, Y.; Liu, W.; Huang, J.; Qiu, S.; Zhong, H.; Liu, D.; Liu, J. Cyclodextrin-Based Metal-Organic Frameworks (CD-MOFs) in Pharmaceutics and Biomedicine. *Pharmaceutics* **2018**, *10* (4), 271.

(6) Gidwani, B.; Vyas, A. A Comprehensive Review on Cyclodextrin-Based Carriers for Delivery of Chemotherapeutic Cytotoxic Anticancer Drugs. *BioMed Res. Int.* **2015**, *2015*, 1−15.

(7) Crini, G. Review: A History of Cyclodextrins. *Chem. Rev.* **2014**, *114* (21), 10940−10975.

(8) Smaldone, R. A.; Forgan, R. S.; Furukawa, H.; Gassensmith, J. J.; Slawin, A. M. Z.; Yaghi, O. M.; Stoddart, J. F. Metalorganic Frameworks from Edible Natural Products. *Angew. Chem., Int. Ed.* **2010**, *49* (46), 8630−8634.

(9) Patyk-Kaźmierczak, E.; Warren, M. R.; Allan, D. R.; Katrusiak, A. Pressure Inverse Solubility and Polymorphism of an Edible γ-Cyclodextrin-Based Metal-Organic Framework. *Phys. Chem. Chem. Phys.* **2017**, *19* (13), 9086−9091.

(10) Forgan, R. S.; Smaldone, R. A.; Gassensmith, J. J.; Furukawa, H.; Cordes, D. B.; Li, Q.; Wilmer, C. E.; Botros, Y. Y.; Snurr, R. Q.; Slawin, A. M. Z.; Stoddart, J. F. Nanoporous Carbohydrate Metal-Organic Frameworks. *J. Am. Chem. Soc.* **2012**, *134* (1), 406−417.

(11) Jackson, K.; Young, D.; Pant, S. Drug-Excipient Interactions and Their Affect on Absorption. *Pharm. Sci. Technol. Today* **2000**, *3* (10), 336−345.

(12) Tamames-Tabar, C.; García-Márquez, A.; Blanco-Prieto, M. J.; Serre, C.; Horcajada, P. MOFs in Pharmaceutical Technology. *Biological and Bio-inspired Nanomaterials*; Springer 2014; pp 83−112.

(13) Chen, G.; Luo, J.; Cai, M.; Qin, L.; Wang, Y.; Gao, L.; Huang, P.; Yu, Y.; Ding, Y.; Dong, X.; Yin, X.; Ni, J. Investigation of Metal-Organic Framework-5 (MOF-5) as an Antitumor Drug Oridonin Sustained Release Carrier. *Molecules* **2019**, *24* (18), 3369.

(14) Liu, J.; Bao, T. Y.; Yang, X. Y.; Zhu, P. P.; Wu, L. H.; Sha, J. Q.; Zhang, L.; Dong, L. Z.; Cao, X. L.; Lan, Y. Q. Controllable Porosity Conversion of Metal-Organic Frameworks Composed of Natural Ingredients for Drug Delivery. *Chem. Commun.* **2017**, *53* (55), 7804−7807.

(15) Tanaka, S. *Mechanochemical Synthesis of MOFs*; Elsevier Inc., 2020.

(16) Krūkle-Bērziņa, K.; Belyakov, S.; Mishnev, A.; Shubin, S. Stability and Phase Transitions of Nontoxic γ-Cyclodextrin-K+ Metal-Organic Framework in Various Solvents. *Crystals* **2020**, *10* (1), 37.

(17) Charpin, P.; Nicolis, I.; Villain, F.; de Rango, C.; Coleman, A. W. β-Cyclodextrin-Potassium Hydroxide-Water (1/1/8). *Acta Crystallogr., Sect. C: Cryst. Struct. Commun.* **1991**, *47* (9), 1829−1833.

(18) Sha, J.-Q.; Wu, L.-H.; Li, S.-X.; Yang, X.-N.; Zhang, Y.; Zhang, Q.-N.; Zhu, P.-P. Synthesis and Structure of New Carbohydrate Metal-Organic Frameworks and Inclusion Complexes. *J. Mol. Struct.* **2015**, *1101*, 14−20.

(19) Bag, P. P.; Kothur, R. R.; Reddy, C. M. Tautomeric Preference in Polymorphs and Pseudopolymorphs of Succinylsulfathiazole: Fast Evaporation Screening and Thermal Studies. *CrystEngComm* **2014**, *16*, 4706.

(20) Sha, J. Q.; Zhong, X. H.; Wu, L. H.; Liu, G. D.; Sheng, N. Nontoxic and renewable metal−organic framework based on α-cyclodextrin with efficient drug delivery. *RSC Adv.* **2016**, *6* (86), 82977−82983.

(21) Koshevoi, E. I.; Samsonenko, D. G.; Dorovatovskii, P. V.; Lazarenko, V. A.; Fedin, V. P. Crystal Structure Of Lithium, Potassium, And Calcium Complexes With B-Cyclodextrine. *J. Struct. Chem.* **2021**, *62* (4), 577−584.

(22) Ding, H.; Wu, L.; Guo, T.; Zhang, Z.; Garba, B. M.; Gao, G.; He, S.; Zhang, W.; Chen, Y.; Lin, Y.; Liu, H.; Anwar, J.; Zhang, J. CD-MOFs Crystal Transformation from Dense to Highly Porous Form for Efficient Drug Loading. *Cryst. Growth Des.* **2019**, *19* (7), 3888−3894.

(23) Sha, J.; Yang, X.; Sun, L.; Zhang, X.; Li, S.; Li, J.; Sheng, N. Unprecedented α-cyclodextrin metal-organic frameworks with chirality: Structure and drug adsorptions. *Polyhedron* **2017**, *127*, 396−402.

(24) Lu, H.; Yang, X.; Li, S.; Zhang, Y.; Sha, J.; Li, C.; Sun, J. Study on a New Cyclodextrin Based Metal−Organic Framework with Chiral Helices. *Inorg. Chem. Commun.* **2015**, *61*, 48−52.

(25) Gassensmith, J. J.; Smaldone, R. A.; Forgan, R. S.; Wilmer, C. E.; Cordes, D. B.; Botros, Y. Y.; Slawin, A. M. Z.; Snurr, R. Q.; Stoddart, J. F. Polyporous Metal-Coordination Frameworks. *Org. Lett.* **2012**, *14* (6), 1460−1463.

(26) Inokuma, Y.; Yoshioka, S.; Ariyoshi, J.; Arai, T.; Fujita, M. Preparation and Guest-Uptake Protocol for a Porous Complex Useful for "crystal-Free" Crystallography. *Nat. Protoc.* **2014**, *9* (2), 246−252.

(27) Dyadkin, V.; Pattison, P.; Dmitriev, V.; Chernyshov, D. A New Multipurpose Diffractometer PILATUS@SNBL. *J. Synchrotron Radiat.* **2016**, *23* (3), 825−829.

(28) Sheldrick, G. M. A Short History of SHELX. *Acta Crystallogr., Sect. A* **2008**, *64* (1), 112−122.

(29) Bourhis, L. J.; Dolomanov, O. V.; Gildea, R. J.; Howard, J. A. K.; Puschmann, H. The Anatomy of a Comprehensive Constrained, Restrained Refinement Program for the Modern Computing Environment - Olex2 Dissected. *Acta Crystallogr., Sect. A: Found. Adv.* **2015**, *71* (1), 59−75.

(30) Macrae, C. F.; Sovago, I.; Cottrell, S. J.; Galek, P. T. A.; McCabe, P.; Pidcock, E.; Platings, M.; Shields, G. P.; Stevens, J. S.; Towler, M.; Wood, P. A. Mercury 4.0: From Visualization to Analysis, Design and Prediction. *J. Appl. Crystallogr.* **2020**, *53* (1), 226−235.

(31) Spek, A. L. Structure Validation in Chemical Crystallography. *Acta Crystallogr., Sect. D: Biol. Crystallogr.* **2009**, *65* (2), 148−155.

(32) Zhang, X.; Chen, Z.; Liu, X.; Hanna, S. L.; Wang, X.; Taheri-Ledari, R.; Maleki, A.; Li, P.; Farha, O. K. A Historical Overview of the Activation and Porosity of Metal-Organic Frameworks. *Chem. Soc. Rev.* **2020**, *49* (20), 7406−7427.

(33) Spackman, P. R.; Turner, M. J.; McKinnon, J. J.; Wolff, S. K.; Grimwood, D. J.; Jayatilaka, D.; Spackman, M. A. CrystalExplorer: a program for Hirshfeld surface analysis, visualization and quantitative analysis of molecular crystals. *J. Appl. Crystallogr.* **2021**, *54* (3), 1006−1011.

(34) Bae, Y.-S.; Yazaydın, A. Ö.; Snurr, R. Q. Evaluation of the BET Method for Determining Surface Areas of MOFs and Zeolites That Contain Ultra-Micropores. *Langmuir* **2010**, *26* (8), 5475−5483.

(35) Ding, J.; Steiner, T.; Saenger, W. Structure of the γ-Cyclodextrin-1-Propanol-17H$_2$O Inclusion Complex. *Acta Crystallogr., Sect. B: Struct. Sci.* **1991**, *47* (5), 731−738.

(36) Steiner, T.; Saenger, W. Channel-Type Crystal Packing in the Very Rare Space Group P 42 1 2 with Z' = 3/4: Crystal Structure of the Complex γ-Cyclodextrin-Methanol- n -Hydrate. *Acta Crystallogr., Sect. B: Struct. Sci.* **1998**, *54* (4), 450−455.

(37) Long, Y.; Yang, L.; Lv, Y.; Liu, Q.; Jin, C.; Zhou, J.; Goodenough, J. B. Crossover from itinerant-electron to localized-electron behavior in $Sr_{1−x}Ca_xCrO_3$ perovskite solid solution. *J. Phys.: Condens. Matter* **2011**, *23* (35), 355601.

(38) Egodawatte, S.; Dominguez, S.; Larsen, S. C. Solvent Effects in the Development of a Drug Delivery System for 5-Fluorouracil Using Magnetic Mesoporous Silica Nanoparticles. *Microporous Mesoporous Mater.* **2017**, *237*, 108−116.